Polymer Chemistry

ROYAL SOCIETY OF CHEMISTRY

PAPER

View Article Online
View Journal | View Issue

Cite this: *Polym. Chem.*, 2023, **14**, 608

Transparent, anti-freezing and highly stretchable solid-state ionic conductors†

Mengdi Zhuang, Yiwen Bao, Juncheng Chen and Hangxun Xu *

Stretchable ionic conductors show great promise for various applications including electronic skins, soft robotics, energy storage devices, actuators, and bio-integrated electronics. Solid-state ionic conductors do not suffer from the dehydration or liquid leakage problems that are typically encountered in hydrogels or ionogels, providing a promising platform for fabricating soft electronics with enhanced stability. However, the design and fabrication of solid-state ionic conductors with high ionic conductivity and excellent mechanical robustness still remain a great challenge. Here, we report a novel synthesis strategy toward the fabrication of solid-state stretchable ionic conductors by seamlessly incorporating layered double hydroxide (LDH) nanosheets into a poly(ionic liquid) (PIL) matrix. In this manner, the LDH nanosheets can form effective electrostatic interactions with the PIL chains, leading to the formation of solid-state ionic conductors with enhanced mechanical strength and toughness without compromising the ionic conductivity. The resultant PIL-LDH composite with an optimal LDH content exhibits high stretchability (>600%), ultra-low temperature tolerance (−81 °C), excellent transparency, and superior ionic conductivity (>3 mS cm^{-1}). Wearable strain and pressure sensors were further demonstrated using the newly developed solid-state ionic conductors to monitor a variety of mechanical deformations with high sensitivity and durability. This study offers a new strategy toward the fabrication of high-performance solid-state ionic conductors for soft and wearable electronics that can stably function under extreme conditions.

Received 19th November 2022,
Accepted 29th December 2022

DOI: 10.1039/d2py01448c

rsc.li/polymers

Introduction

Natural living organisms utilize ions to transduce signals perceived from external stimuli.[1] This unique feature has inspired the development of soft ionic conductors that can transport electric currents using mobile ions.[2–5] Soft ionic conductors provide unique characteristics of stretchability, transparency, ionic conductivity, and even the anti-freezing property that are challenging to achieve by conventional electronic conductors.[4–6] Consequently, ionic conductors exhibit great potential in a wide range of applications such as electronic skins, bio-integrated electronics, electroluminescent devices, capacitive touchpads, and soft robotics.[7–11] Hydrogels and ionogels are two classes of polymer materials that have been extensively investigated in fabricating stretchable ionic conductors.[12–14] However, hydrogels are prone to dehydration due to the evaporation of water and may freeze at subzero temperatures, severely limiting their practical applications in soft electronics.[15] Meanwhile, using a large amount of solvents often leads to compromised mechanical properties.[16] On the other hand, stretchable ionogels also suffer from the liquid leakage problem under mechanical deformations, resulting in reduced ionic conductivity.[17] Moreover, the biocompatibility and biotoxicity of ionic liquids in ionogels still remain a major concern for application in wearable electronics.[18] Therefore, solid-state and liquid-free ionic conductors without any liquid in the polymer network are highly desirable as alternative ionic conductors toward the fabrication of various soft electronics with enhanced durability.

Compared with gel-based ionic conductors, however, the ionic conductivity of solid-state ionic conductors requires further enhancement due to the much slower mobility of charged polymer chains in the solid state.[19–21] In addition, the mechanical strength of current solid-state ionic conductors also needs to be further improved without compromising the ionic conductivity.[22] Furthermore, very few of them show the anti-freezing property for potential applications at subzero temperatures.[23] Consequently, it still remains a great challenge to develop solid-state ionic conductors with excellent ionic conductivity, high mechanical strength, and ultra-low temperature tolerance.

Poly(ionic liquid)s (PILs) are inherently ion-conducting polymers with repeated ionic liquid species in the polymer

Collaborative Innovation Center of Chemistry for Energy Materials (iChEM), Department of Polymer Science and Engineering, University of Science and Technology of China, Hefei, Anhui 230026, China. E-mail: hxu@ustc.edu.cn

† Electronic supplementary information (ESI) available. See DOI: https://doi.org/10.1039/d2py01448c

chains.[24–27] They exhibit high ionic conductivity, excellent thermal and electrochemical stability, and superior structural tunability. Meanwhile, PILs typically display much lower glass transition temperatures (T_g) than other ion-containing polymers.[26,27] Therefore, they are very promising for the fabrication of stretchable ionic conductors with the anti-freezing property.[28,29] Generally, a low T_g is beneficial for enhancing the ionic conductivity.[27,30] However, this feature would also result in undesirable mechanical performances.[31] Central to addressing the tradeoff between the ionic conductivity and mechanical robustness of solid-state ionic conductors is to introduce nanofillers into the ionic polymer network without compromising the ionic conductivity. Thus far, metal oxides, silicas, and carbon materials have been used to fabricate PIL-based composites.[32] Unfortunately, these composites typically exhibit poor transparency. More importantly, the molecular interactions between the nanofillers and polymers are generally very weak, thereby inevitably resulting in impeded ionic transport. In this context, new nanofillers that can be seamlessly incorporated into the polymer matrix are highly desirable.

Layered double hydroxides (LDHs) are a type of two-dimensional (2D) intercalation compound comprising positively charged hydroxide layers with exchangeable interlayer anions.[33,34] In light of the charge-bearing nature of LDHs, they hold great promise toward the fabrication of solid-state ionic conductors. Here, we report a facile approach for the preparation of solid-state ionic conductors *via* establishing effective electrostatic interactions between the PILs and exfoliated LDH nanosheets. We first employed an ion exchange strategy to intercalate polymerizable anions into the interlayers of bulk LDHs. Subsequently, these expanded LDHs were exfoliated in ionic liquid monomers to form homogenous suspensions which can directly form solid-state ion-conducting composites by a photopolymerization process. In this manner, the LDH nanosheets are homogeneously distributed in the polymer matrix and the resultant PIL-LDH composites are highly transparent. They exhibit high stretchability (>600%) with high ionic conductivity (3.3 mS cm^{-1} at 25 °C). In addition, the as-prepared solid-state ionic conductors are highly resilient and display significantly improved mechanical strength and fracture toughness compared with pure PILs. More importantly, these solid-state conductors can maintain high ionic conductivity and stretchability even at ultra-low temperatures. Wearable strain and pressure sensors were further demonstrated using the newly developed solid-state ionic conductors to detect a variety of mechanical deformations with high sensitivity and durability. Our study offers a facile yet effective approach toward the rational design of solid-state ionic conductors that can stably function under extreme conditions, representing a hallmark to develop more exciting ion-conducting polymers for soft and wearable electronics moving forward.

Results and discussion

The PIL-LDH composites were prepared through incorporating LDH nanosheets into the PIL matrix followed by *in situ* photopolymerization. The entire fabrication process is schematically illustrated in Fig. 1a. The chemical structures of the paired cations and anions of the ionic liquid monomers are critical in determining the T_g and ionic conductivity of the PILs. We first synthesized a new ionic liquid monomer (1-butyl-3-methyl imidazolium (3-sulfopropyl) acrylate, [BMIM][SPA]) containing both imidazole and sulfonate ions (Fig. S1†). Meanwhile, MgAl-LDH was chosen as the nanofiller owing to its high conductivity among various LDHs.[35] We found that, during the

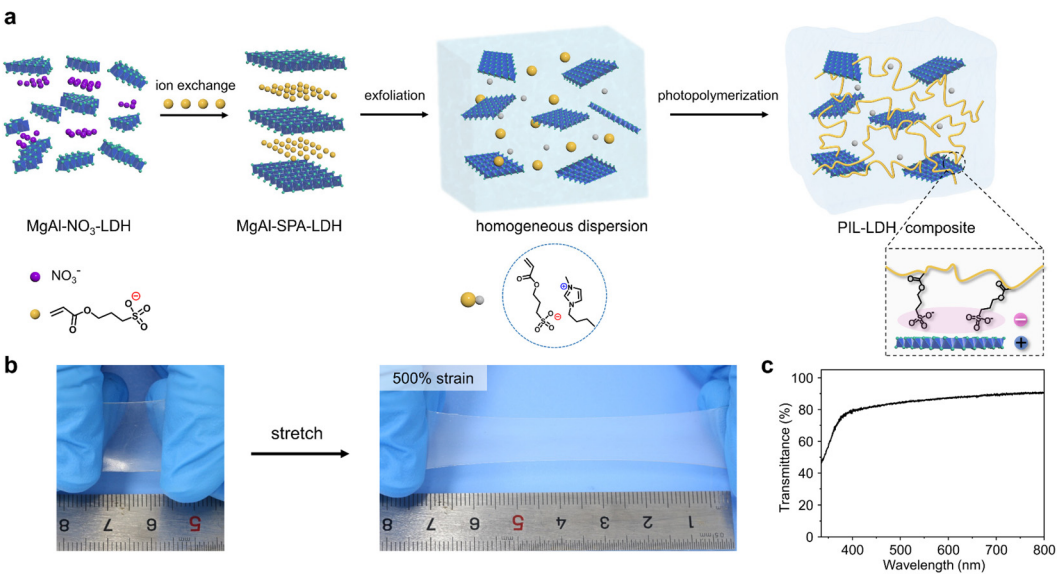

Fig. 1 (a) Schematic showing the preparation process of the PIL-LDH composites. (b) Optical images of the as-obtained PIL-LDH composite before and after stretching (the LDH content is 10 wt%). (c) UV-vis transmittance spectrum of the as-fabricated PIL-LDH composite containing 10 wt% LDH.

synthesis of MgAl-LDH, the nitrate anions (NO_3^-) can be effectively replaced by the sulfonate ions (SPA) *via* the ion exchange mechanism. Powder X-ray diffraction (PXRD) patterns revealed that the interlayer distance of the MgAl-LDH markedly increased from 0.77 nm to 1.82 nm after the ion exchange process (Fig. S2†), reflecting that the SPA anions were successfully intercalated into the LDHs. Fourier transform infrared (FTIR) spectroscopy measurements indicated that the peak at 1384 cm^{-1} corresponding to the nitrate anions completely disappeared after the ion exchange process whereas the characteristic peaks of the SPA anions and the acrylate moieties emerged (Fig. S3a†). Meanwhile, an obvious shift to a higher frequency of the SO_3^- symmetric stretching band from 1040 to 1048 cm^{-1} can be observed in the intercalated LDHs (Fig. S3b†), implying that the SPA anions can form effective electrostatic interactions with the positively charged LDHs.[36] Consequently, the LDHs intercalated with SPA anions can be easily exfoliated into LDH nanosheets by a simple ultrasonication process as a result of significantly enlarged interlayer distances, leading to a homogeneous dispersion consisting of exfoliated LDH nanosheets and ionic liquid monomers (Fig. S4 and S5†). Subsequently, highly stretchable PIL-LDH composites can be obtained *via* photopolymerization under UV light irradiation (Fig. 1b). In this approach, PIL-LDH composites with different shapes can be prepared (Fig. S6†). The as-obtained PIL-LDH composites are highly transparent. For example, the PIL-LDH composite containing 10 wt% LDH exhibits a transparency of ~88% at 600 nm, whereas the transparency of the pure PIL film is ~93% (Fig. 1c and S7†). This observation indicates that the LDH nanosheets are uniformly dispersed inside the PIL matrix to achieve transparent and stretchable PIL-LDH composites.

As shown in Fig. 2a, transmission electron microscopy (TEM) characterization of the PIL-LDH composite containing 10 wt% LDH nanosheets *via* cryo-ultramicrotomy clearly reveals that the exfoliated LDH nanosheets are homogeneously distributed in the PIL matrix. In addition, XRD characterization was used to reveal the distribution of LDH nanosheets inside the PIL matrix. The XRD patterns shown in Fig. S8† reveal that the strong and sharp diffraction peaks related to the ordered structure of bulk LDHs completely disappear in the PIL-LDH composites, indicating that the LDHs are fully exfoliated into nanosheets and homogeneously distributed inside the PIL matrix.[37] Cross-sectional scanning electron microscopy (SEM) and the corresponding elemental mapping results further confirmed that the LDH nanosheets were uniformly dispersed inside the polymer matrix (Fig. S9†). These results conclusively demonstrate that the synthetic strategy developed in this study can result in stretchable and transparent PIL-LDH composites with homogeneously distributed LDH nanosheets.

Since the surfaces of the exfoliated LDH nanosheets are inherently bearing positive charges, they can effectively form electrostatic interactions with PILs. X-ray photoelectron spectroscopy (XPS) measurements revealed that the high resolution S 2p spectrum of the PILs can be deconvoluted into two peaks at 168.31 and 167.11 eV, ascribed to the presence of the sulfonate groups in the PIL (Fig. 2b). These peaks slightly shifted to higher binding energies at 168.40 and 167.24 eV due to the formation of electrostatic interactions between the exfoliated LDH nanosheets and the PIL chains as schematically shown in Fig. 1a.[38] In addition, the Raman spectra shown in Fig. 2c indicate that the peak corresponding to the symmetric stretching of the sulfonate groups shifts to a higher frequency from 1041.4 cm^{-1} in the pure PIL film to 1042.1 cm^{-1} after the formation of the PIL-LDH composite, further confirming that the electrostatic interactions between the positively charged LDH nanosheets and sulfonate groups in PIL are well established.[39] These characterization studies unambiguously confirm that the synthetic route reported here can successfully form strong electrostatic interactions between PIL and exfoliated LDH nanosheets. Therefore, the LDH nanosheets in fact can serve as non-covalent crosslinkers inside the PIL matrix, which is beneficial for enhancing the mechanical performance of the composites.

The LDH nanosheets play a critical role in enhancing the mechanical performance of the PIL-LDH composites. Fig. 3a shows the tensile stress–strain curves of PIL-LDH composites with different contents of the LDH nanosheets. The maximum elongation at break of the pure PIL film was 800% but the

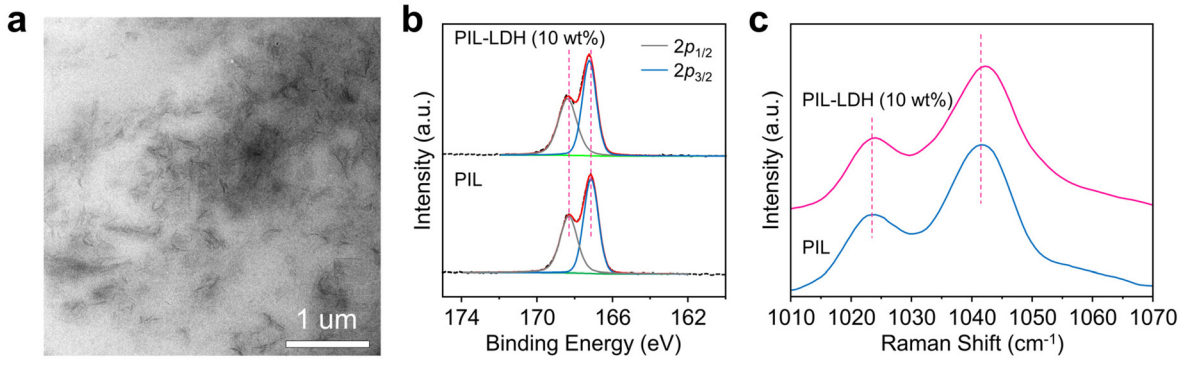

Fig. 2 (a) TEM image of the PIL-LDH composite containing 10 wt% LDH. (b) High-resolution S 2*p* XPS spectra and (c) Raman spectra of the PIL and PIL-LDH composite containing 10 wt% LDH.

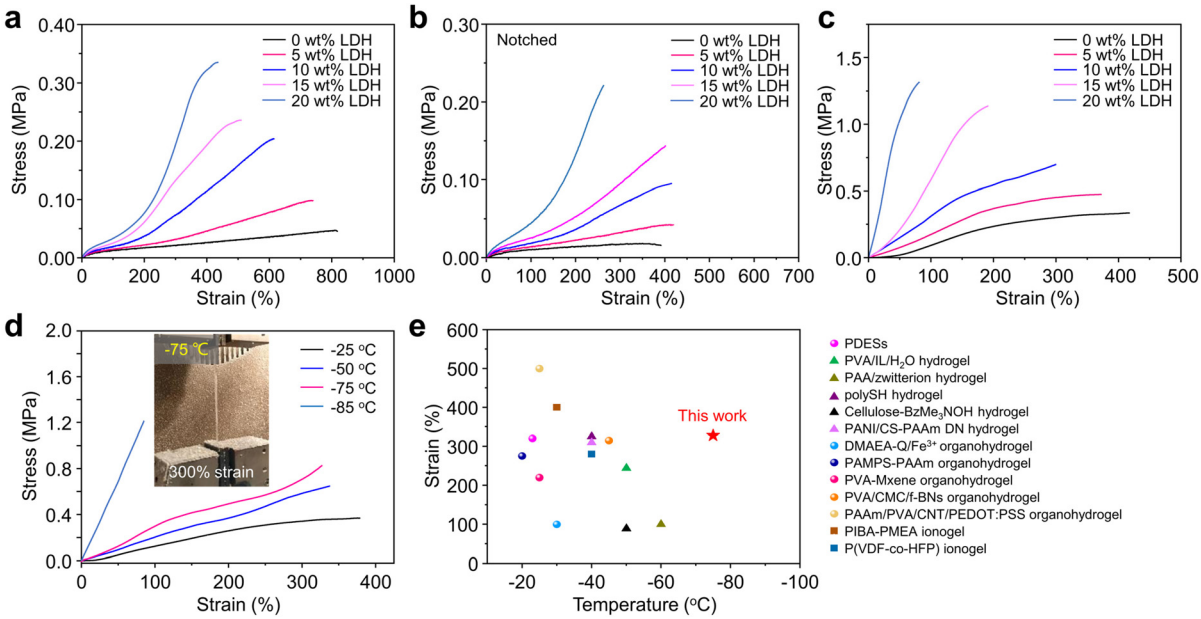

Fig. 3 Tensile stress–strain curves of the PIL-LDH composites with different LDH contents (a) before and (b) after being notched at room temperature. (c) Tensile stress–strain curves of the PIL-LDH composites with different LDH contents measured at −65 °C. (d) Tensile stress–strain curves of the PIL-LDH composite with 10 wt% LDH measured at different temperatures. The inset shows the photograph of the sample stretched to 300% strain at −75 °C. (e) Comparison of the anti-freezing performance of various stretchable ionic conductors summarized from recent reports.

maximum stress at break was limited to 0.047 MPa at room temperature. After introducing LDH nanosheets into the PIL matrix, the mechanical strengths of the stretchable composites gradually increased. The ultimate stress of the PIL-LDH composite with 20 wt% LDH nanosheets remarkably increased to 0.34 MPa owing to the strengthening effect of the homogeneously distributed LDH nanosheets. Notably, the maximum elongation at break was still over 400% when the content of the LDH nanosheets was up to 20 wt%. Meanwhile, the Young's modulus could reach 0.08 MPa with 20 wt% LDH (Table S1†). The resilience of the PIL-LDH composites was evaluated by cyclic tensile tests. Obviously, the PIL-LDH composites with different LDH contents can be stretched up to 500% strain without fracture and then their original shapes can be recovered after releasing without notable decays (Fig. S10†). Moreover, the successive loading–unloading cycling tests at strains of 100%, 300%, and 500% revealed that these composites exhibited negligible permanent deformations after the first loading–unloading cycle (Fig. S11†). During the first cycle, irreversible realignment of the LDH nanosheets or noncovalent bond dissociation such as detachment of polymer chains from LDH nanosheets may occur, resulting in a residual strain of 10%. However, owing to the restoration of electrostatic interactions, the PIL-LDH composites exhibit good resilience and fatigue resistance during the following loading–unloading cycles. Thus, the PIL-LDH composites are highly elastic with excellent resilience and fatigue resistance due to the efficient dissociation–reassociation nature of the dynamic and non-covalent electrostatic interactions in the polymer network.[40]

We further assessed the toughness of the PIL-LDH composites with different LDH contents using the standard tensile strength test on notched samples (Fig. 3b). After notching, the maximum strain of the pure PIL film markedly reduced from 800% to less than 400% with a fracture toughness of 0.25 kJ m^{-2}, indicating that the pure PIL film exhibits very poor fracture toughness. In sharp contrast, the fracture toughness of the notched PIL-LDH composite with 20 wt% LDH was dramatically enhanced to 1.72 kJ m^{-2} which is about 6 times higher than that of the pure PIL film (Fig. S12†). Moreover, the incorporation of the exfoliated LDH nanosheets into the PIL matrix can effectively prevent the extension of the created notch under tensile loading (Fig. S13†). We also prepared a PIL-LDH composite by directly mixing unexfoliated LDHs into PILs and measured the corresponding mechanical properties (Fig. S14†). Obviously, the PIL-LDH composites fabricated by our strategy exhibited not only excellent resilience and fatigue resistance, but also significantly enhanced Young's modulus and fracture toughness, likely attributing to the strong interfacial electrostatic interactions between the exfoliated LDH nanosheets and the PIL matrix.[41] These findings strongly suggest that our strategy can successfully improve the mechanical performances of stretchable ion-conducting conductors.

Stretchable PILs are intrinsically capable of maintaining the ionic conductivity in ultra-cold environments (*i.e.*, anti-freezing characteristics). Nevertheless, the incorporation of inorganic fillers into the ion-conducting polymer networks usually increases the T_g, which may impede their potential application at subzero temperatures. To assess the anti-freezing property of the PIL-LDH composites, differential scanning

calorimetry (DSC) measurements of the PIL-LDH composites were conducted. It turned out that the T_g of the PIL-LDH composite containing 10 wt% LDH could remain at −81 °C which was only 0.6 °C higher than that of the pure PIL (Fig. S15†). Moreover, the T_g of the PIL-LDH composite was still below −76 °C when the content of the LDH nanosheets further increased to 20 wt%. The subtle increase in T_g could be caused by the adsorption of polymer chains on the surface of LDH nanosheets *via* electrostatic interactions. Therefore, the PIL-LDH composites with low T_g could exhibit a superior anti-freezing property. Accordingly, as shown in Fig. 3c, these PIL-LDH composites exhibit excellent stretchability even at −65 °C. The PIL-LDH composite with 10 wt% LDH still retained a high stretchability of more than 300% even at −75 °C and became rigid only when the temperature decreased below T_g (−81 °C). In addition, the stretchability of the PIL-LDH composites is fully recoverable even under repeated stretching at 100% strain (Fig. S16†). Such outstanding stretchability at ultra-cold temperatures has surpassed most of the stretchable anti-freezing ionic conductors reported previously (Fig. 3e and Table S2†). Therefore, the PIL-LDH composites developed here not only exhibit excellent elasticity with improved toughness, but also possess outstanding anti-freezing property.

The newly developed PIL-LDH composites also exhibit excellent ionic conductivity. As shown in Fig. 4a, before incorporating LDH nanosheets, the pure PIL film inherently exhibits an ionic conductivity of 3.65 mS cm^{-1}. The ionic conductivity of the PIL-LDH composites decreases with increasing LDH contents to about 2.65 mS cm^{-1} for the PIL-LDH composite with 20 wt% LDH. The slight decrease in the ionic conductivity can be ascribed to the partially impeded ion transport by the LDH nanosheets inside the PIL network. The ionic conductivity can be enhanced by increasing the temperature. For example, the ionic conductivity of the PIL-LDH composite with 10 wt% LDH could increase from 3.3 mS cm^{-1} to over 10 mS cm^{-1} when the temperature increases from 25 °C to 50 °C (Fig. 4b). More importantly, the stretchable PIL-LDH conduc-

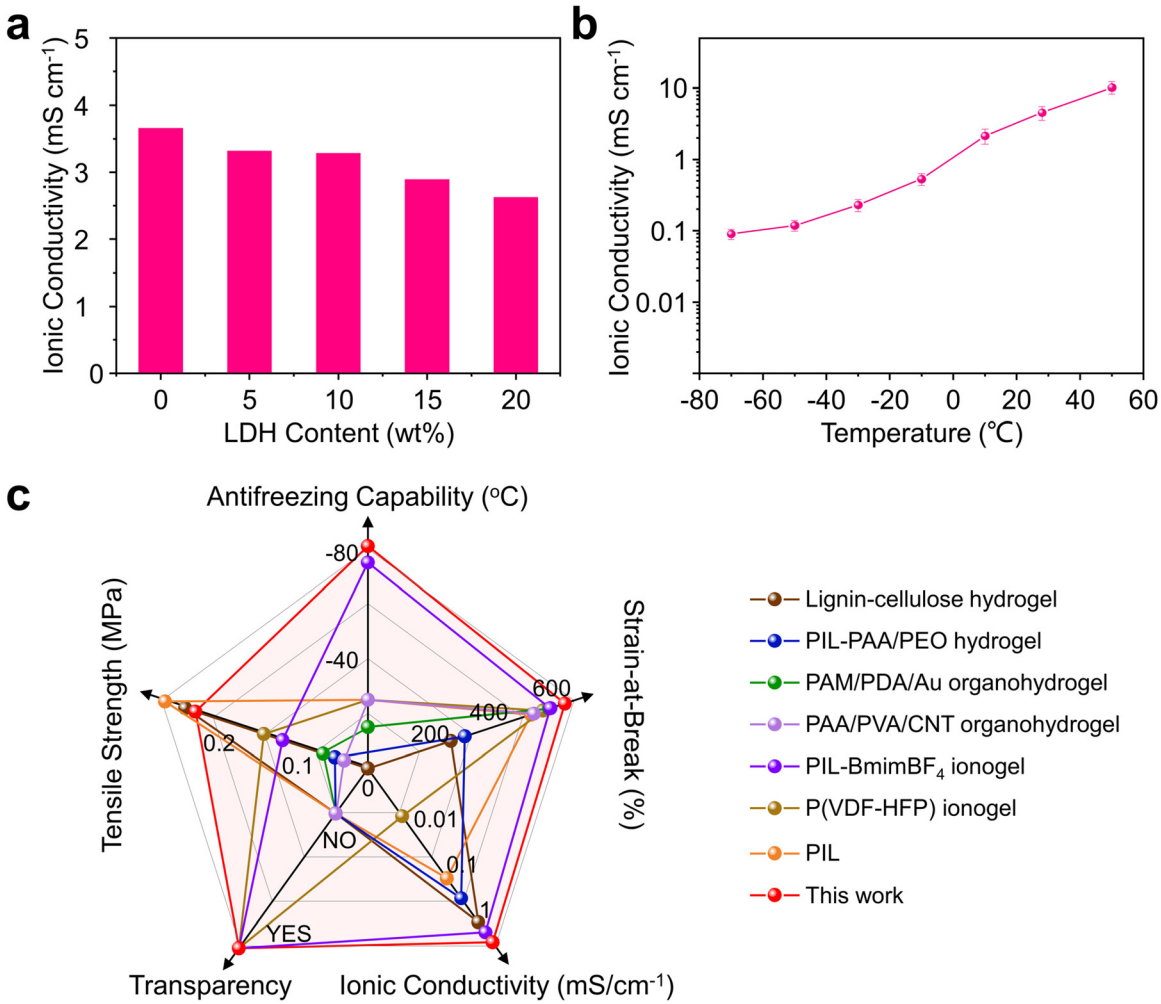

Fig. 4 (a) Measured ionic conductivities of the PIL-LDH composites as a function of the LDH content. (b) The dependence of the ionic conductivity of the PIL-LDH composite containing 10 wt% LDH on the temperature. (c) Comprehensive comparison of the properties of the PIL-LDH composites with recently reported stretchable ionic conductors.

tors reported here also exhibit promising ionic conductivity even at subzero temperatures. The measured ionic conductivity of the PIL-LDH composite with 10 wt% LDH was about 0.1 mS cm^{-1} at an ultra-low temperature of −70 °C. The ionic conductivity and anti-freezing performance of the PIL-LDH composites have surpassed most of the stretchable solid-state ionic conductors reported to date (Table S3†). Thus, compared with other state-of-the-art soft ionic conductors, the PIL-LDH composites reported here exhibit much superior mechanical performance, ionic conductivity, and anti-freezing property (Fig. 4c and Table S4†).

The PIL-LDH composites reported here are highly stretchable and exhibit prominent ionic conductivity at ultra-cold temperatures, enabling the fabrication of flexible electronics for potential use at subzero temperatures. The relative resistance change ($\Delta R/R_0$) ($\Delta R/R_0 = (R - R_0)/R_0$; R_0 and R represent the resistance at the original shape and after stretching, respectively) of the PIL-LDH composite containing 10 wt% LDH was first evaluated at both room temperature and −65 °C. The gauge factor (GF), which is defined as the slope of the ($\Delta R/R_0$) *versus* strain plot, is a key parameter to describe the sensitivity of strain sensors. The as-fabricated strain sensor displayed a monotonic increase in resistance at room temperature (Fig. S17†). The measured GF was 4.57, which is superior to most of the stretchable ionic conductors reported to date (Table S5†). When the temperature was decreased to −65 °C, the measured GF was 2.42 within 150% strain and this value further increased to 5.54 for strains beyond 150% (Fig. 5a), indicating that the strain sensor based on the PIL-LDH composite could exhibit high sensitivity with a broad temperature range. Moreover, the as-fabricated strain sensor displayed excellent durability while being repeatedly stretched up to 200% strain for 1000 cycles under −65 °C (Fig. S18†). The strain sensor was then attached to a prosthetic hand and used to monitor joint movements with obvious resistance changes under ultra-cold conditions. As shown in Fig. 5b, when the finger is progressively bent from 0° to 90°, the relative resistance change increases instantaneously in response to the finger movement in a step-by-step manner. When the finger moves back to the original position, the relative resistance changes also return to the original values, indicating that the strain sensor can accurately detect various movements when it is used in wearable electronics. More importantly, as displayed in Fig. 5c, the strain sensor exhibits excellent durability during repeated bending as negligible variation in relative resistance can be observed.

In addition to the piezoresistive sensing, the resultant PIL-LDH composites can be further developed as pressure sensors based on the capacitive sensing mode. Fig. 5d shows the relative change in capacitance ($\Delta C/C_0$) of the pressure sensor at −65 °C as a function of applied pressure. The relative capacitance can sensitively increase in accordance with the applied pressure. The sensitivity is 0.76 kPa^{-1} in the relatively low pressure range (0–6 kPa) and drops to 0.38 kPa^{-1} as the pressure increases from 6 kPa to 25 kPa. This variation in sensitivity might be ascribed to the structural change under

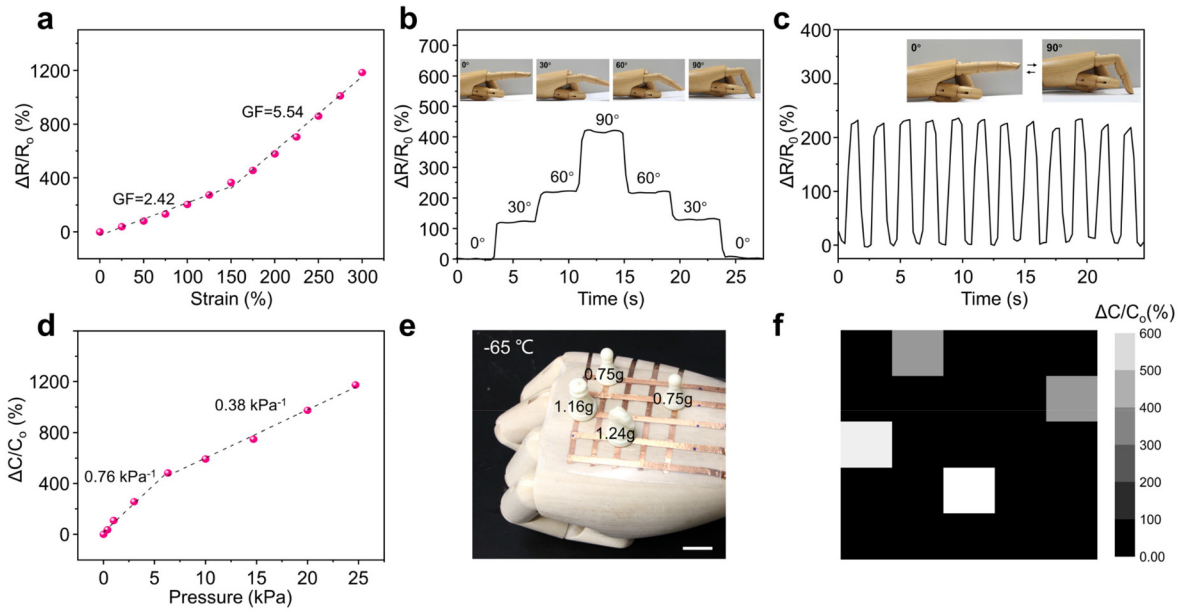

Fig. 5 (a) Relative resistance changes of the PIL-LDH composite containing 10 wt% LDH as a function of applied strain measured at −65 °C. (b) Relative resistance changes of the PIL-LDH composite containing 10 wt% LDH in response to the bending of the finger at −65 °C. (c) Temporal variations of relative resistance changes in response to repeated bending of the finger at −65 °C. (d) Relative capacitance changes of the PIL-LDH composite containing 10 wt% LDH as a function of the applied pressure at −65 °C. (e) The photograph showing four mini chess pieces distributed on the pressure sensor array attached to the back of a prosthetic hand at −65 °C (scale bar = 10 mm) and (f) corresponding signal map showing the pressure distribution in (e).

different compressive deformations.[42] The excellent pressure sensing performance of the PIL-LDH composites along with the unique anti-freezing property makes them ideal candidates for practical pressure sensing at subzero temperatures. In addition, for practical applications, it is highly desirable to fabricate pressure sensors in an array configuration with multiple pixels to spatially discern pressure distributions. Here, as shown in Fig. 5e, a 5 × 5 pixel array was fabricated by using the PIL-LDH composite. Fig. 5f shows that the response of the integrated sensor array to the locations of four mini chess pieces with different weights (2 Pawns of 0.75 g, a King of 1.24 g and a Queen of 1.16 g,) can be precisely detected by the pressure sensor array at −65 °C. Therefore, the PIL-LDH composites developed in this study exhibit extraordinary mechanical, electrical, and anti-freezing characteristics for both strain and pressure sensing, even under ultra-cold conditions.

Conclusions

In summary, we have demonstrated that introducing LDH nanosheets into an ionic polymer network can successfully address the tradeoff between the ionic conductivity and mechanical robustness in solid-state ionic conductors. The exfoliated LDH nanosheets can homogeneously disperse inside the PIL matrix to form stretchable solid-state ionic conductors. The dynamic non-covalent crosslinking between exfoliated LDH nanosheets and PIL chains *via* effective electrostatic interactions results in ionic conductors with excellent resilience and much enhanced mechanical strength and fracture toughness. Moreover, the PIL-LDH composites exhibit desirable transparency, high stretchability, excellent ionic conductivity, and prominent anti-freezing property. We further demonstrated that these composites can be fabricated as strain and pressure sensors with high sensitivity and excellent stability. The design and fabrication strategy presented in this study would be very meaningful for future development of solid-state ion-conducting elastomers with robust mechanical and electrical performances.

Conflicts of interest

There are no conflicts of interest to declare.

Acknowledgements

This work was partially carried out at the USTC Center for Micro- and Nanoscale Research and Fabrication. This work was supported by the National Key Research and Development Program of China (2021YFA1500800), the CAS Project for Young Scientists in Basic Research (YSBR-004), the National Natural Science Foundation of China (52225307 and 22105193), and the Fundamental Research Funds for the Central Universities (20720220007 and 20720220011).

References

1 C. H. Yang and Z. G. Suo, *Nat. Rev. Mater.*, 2018, **3**, 125–142.
2 C. Keplinger, J. Sun, C. C. Foo, P. Rothemund, G. M. Whitesides and Z. Suo, *Science*, 2013, **341**, 984–987.
3 C. Wan, K. Xiao, A. Angelin, M. Antonietti and X. Chen, *Adv. Intell. Syst.*, 2019, **1**, 1900073.
4 H. R. Lee, C. C. Kim and J. Y. Sun, *Adv. Mater.*, 2018, **30**, 1704403.
5 H. Chun and T. D. Chung, *Annu. Rev. Anal. Chem.*, 2015, **8**, 441–462.
6 Y. Jian, S. Handschuh-Wang, J. Zhang, W. Lu, X. Zhou and T. Chen, *Mater. Horiz.*, 2021, **8**, 351–369.
7 W. Zhang, B. Wu, S. Sun and P. Wu, *Nat. Commun.*, 2021, **12**, 4082.
8 Y. J. Jo, H. Kim, J. Ok, Y.-J. Shin, J. H. Shin, T. H. Kim, Y. Jung and T. I. Kim, *Adv. Funct. Mater.*, 2020, **30**, 1909707.
9 H. D. Xuan, B. Timothy, H. Y. Park, T. N. Lam, D. Kim, Y. Go, J. Kim, Y. Lee, S. I. Ahn, S. H. Jin and J. Yoon, *Adv. Mater.*, 2021, **33**, 2008849.
10 C. C. Kim, H. H. Lee, K. H. Oh and J. Y. Sun, *Science*, 2016, **353**, 682–687.
11 T. Li, G. Li, Y. Liang, T. Cheng, J. Dai, X. Yang, B. Liu, Z. Zeng, Z. Huang and Y. Luo, *Sci. Adv.*, 2017, **3**, e1602045.
12 Z. Lei, Q. Wang, S. Sun, W. Zhu and P. Wu, *Adv. Mater.*, 2017, **29**, 1700321.
13 Z. Lei and P. Wu, *Nat. Commun.*, 2018, **9**, 1134.
14 T. Q. Li, Y. T. Wang, S. H. Li, X. K. Liu and J. Q. Sun, *Adv. Mater.*, 2020, **32**, 2002706.
15 D. Zhou, F. Chen, S. H. Wang, T. Gan, X. Zhou and X. Zhou, *ChemPhysChem*, 2019, **20**, 2139–2154.
16 N. R. Richbourg and N. A. Peppas, *Prog. Polym. Sci.*, 2020, **105**, 101243.
17 Z. Lei and P. Wu, *Nat. Commun.*, 2019, **10**, 3429.
18 B. Kudlak, K. Owczarek and J. Namiesnik, *Environ. Sci. Pollut. Res.*, 2015, **22**, 11975–11992.
19 L. Shi, T. Zhu, G. Gao, X. Zhang, W. Wei, W. Liu and S. Ding, *Nat. Commun.*, 2018, **9**, 2630.
20 X. Qu, W. Niu, R. Wang, Z. Li, Y. Guo, X. Liu and J. Sun, *Mater. Horiz.*, 2020, **7**, 2994–3004.
21 P. Zhang, W. Guo, Z. H. Guo, Y. Ma, L. Gao, Z. Cong, X. J. Zhao, L. Qiao, X. Pu and Z. L. Wang, *Adv. Mater.*, 2021, **33**, 2101396.
22 B. Yiming, Y. Han, Z. Han, X. Zhang, Y. Li, W. Lian, M. Zhang, J. Yin, T. Sun, Z. Wu, T. Li, J. Fu, Z. Jia and S. Qu, *Adv. Mater.*, 2021, **33**, 2006111.
23 R. A. Li, T. Fan, G. Chen, K. Zhang, B. Su, J. Tian and M. He, *Chem. Mater.*, 2020, **32**, 874–881.
24 M. Armand, F. Endres, D. R. MacFarlane, H. Ohno and B. Scrosati, *Nat. Mater.*, 2009, **8**, 621–629.
25 D. Mecerreyes, *Prog. Polym. Sci.*, 2011, **36**, 1629–1648.
26 J. Yuan, D. Mecerreyes and M. Antonietti, *Prog. Polym. Sci.*, 2013, **38**, 1009–1036.
27 W. Qian, J. Texter and F. Yan, *Chem. Soc. Rev.*, 2017, **46**, 1124–1159.

28 Y. Ren, J. Guo, Z. Liu, Z. Sun, Y. Wu, L. Liu and F. Yan, *Sci. Adv.*, 2019, **5**, eaax0648.
29 Z. Liu, Y. Wang, Y. Ren, G. Jin, C. Zhang, W. Chen and F. Yan, *Mater. Horiz.*, 2020, **7**, 919–927.
30 Z. Wojnarowska, H. Feng, Y. Fu, S. Cheng, B. Carroll, R. Kumar, V. N. Novikov, A. M. Kisliuk, T. Saito, N.-G. Kang, J. W. Mays, A. P. Sokolov and V. Bocharova, *Macromolecules*, 2017, **50**, 6710–6721.
31 T. C. Rhoades, J. C. Wistrom, R. D. Johnson and K. M. Miller, *Polymer*, 2016, **100**, 1–9.
32 S. Zhang, Q. Zhuang, M. Zhang, H. Wang, Z. Gao, J. Sun and J. Yuan, *Chem. Soc. Rev.*, 2020, **49**, 1726–1755.
33 Q. Wang and D. O'Hare, *Chem. Rev.*, 2012, **112**, 4124–4155.
34 J. Yu, Q. Wang, D. O'Hare and L. Sun, *Chem. Soc. Rev.*, 2017, **46**, 5950–5974.
35 P. Sun, R. Ma, X. Bai, K. Wang, H. Zhu and T. Sasaki, *Sci. Adv.*, 2017, **3**, e1602629.
36 V. Deimede, V. Voyiatzis, J. K. Kallitsis, L. Qingfeng and N. J. Bjerrum, *Macromolecules*, 2000, **33**, 7609–7617.
37 R. Z. Ma and T. Sasaki, *Adv. Mater.*, 2010, **22**, 5082–5104.
38 T. B. Taketa, D. M. dos Santos, A. Fiamingo, J. M. Vaz, M. M. Beppu, S. P. Campana-Filho, R. E. Cohen and M. F. Rubner, *Langmuir*, 2018, **34**, 1429–1440.
39 Y. Fan and C. J. Cornelius, *J. Mater. Sci.*, 2013, **48**, 1153–1161.
40 T. Long, Y. Li, X. Fang and J. Sun, *Adv. Funct. Mater.*, 2018, **28**, 1804416.
41 X. H. Wang, S. N. Zhan, Z. Y. Lu, J. Li, X. Yang, Y. N. Qiao, Y. F. Men and J. Q. Sun, *Adv. Mater.*, 2020, **32**, 2005759.
42 X. Zhang, N. Sheng, L. Wang, Y. Tan, C. Liu, Y. Xia, Z. Nie and K. Sui, *Mater. Horiz.*, 2019, **6**, 326–333.